Manufacturing nanostructured YSZ coatings by suspension plasma spraying (SPS): effect of injection parameters

E Meillot, R Vert, C Caruyer, D Damiani, Michel Vardelle

Manufacturing nanostructured YSZ coatings by suspension plasma spraying (SPS): Effect of injection parameters.

E. Meillot[(1)], R. Vert[(1)], C. Caruyer[(1)], D. Damiani[(1)], M. Vardelle[(2)]

(1) CEA, DAM, Le Ripault, F−37260, Monts, France

(2) SPCTS − UMR CNRS 6638, ENSIL, University of Limoges, France

Corresponding author : Erick Meillot. erick.meillot@cea.fr

Abstract. The suspension plasma spraying process is investigated by using shadow imaging techniques to appreciate the different trajectories of the liquid jet interacting with a DC high-energy plasma flow. Then, the modelling of different liquid injections (isolated droplet, train of droplets and continuous jet) helps to determine which injection type must be preferred. From that, coating depositions have been carried out with yttria zirconia suspension. Trajectory deviations at impact have been measured depending on the injection pressure and injection location. Coatings have been realized under the same operating investigations and their microstructures and mechanical properties have been characterized.

Key words: suspension plasma spraying, shadow imaging, coating, trajectory deviation, mechanical properties, hardness, nano indentation, micro Vickers.

1. Introduction

Surface treatment processes allow the deposition of various materials on manufacturing parts to improve their properties. Among them, plasma spraying is well adapted to ceramic coating deposition. The conventional plasma spraying uses micrometer size powder, injected with a carrier gas into the plasma plume, to produce thick layers, generally from 100 µm to close or more than the millimeter. To decrease the thickness of coatings, smaller size powders could be used, for instance nano size materials. In this case, the small particle mass requires the use of liquid medium, like water or ethanol, to increase the particle momentum.and ensure their penetration into the plasma jet. The nano particles are put in suspension and pushed to the plasma jet by pressure via an injector close to the torch exit. After evaporation of the medium, the particles are treated in the plasma plume and impact the substrate and so generate a coating by piling up of lamellae.

Such deposition process appears as good candidate for thermal barrier coatings. In the context of the next generation of nuclear energy systems selected by the Generation IV International Forum, studies **[1]** have been engaged to determine and develop materials as first insulating wall capable of

operating under high temperatures (over 850°) and resisting at high pressure variations and wear (7 MPa of helium flow).

In this paper, investigations upon introduction of YSZ (Yttria-Stabilized Zirconia) suspension into DC plasma flow are presented. After a short description of the operating parameters, interactions of water jet with the plasma plume is described by two ways (numerical and experimental). Then, coatings are realized and characterized through their microstructures and properties. The first characterizations concern the mechanical coating properties to determine their wear behavior to the high pressure helium flow.

2. Operating conditions.

The plasma spraying conditions are summarized in **Table 1**, while the injection positions are represented in **Figure 1**. The choice of a high flow rate of Argon/Hydrogen/helium mixture and the high current intensity comes from the requirement of high velocity and temperature to get dense coatings **[2]**. However, the use of hydrogen involves a modification of the electrical arc behaviour in the torch, from a takeover mode to a restrike one due to the erratic arc root movement at the anode wall **[3]**, **[4]**. This fact implies that the downstream plasma flow is not stable but presents stretching and shrinking with hot gas puffs and modification of the gas velocity. These instabilities lead to different liquid treatments depending on the instantaneous state of the plasma **[5]** with more or less penetration of the liquid in the jet.

Plasma torch	Suler-Metco F4-VB
Nozzle diameter (mm)	6
Plasma gas mixture	$Ar/He/H_2$
Plasma gas flow rate (slpm)	45/45/3
Arc current intensity (A)	700
Plasma effective power (kW)	31 ± 0.2
Specific enthalpy (MJ/kg)	21.4
Injector diameter (µm)	250

Table 1: Plasma operating conditions

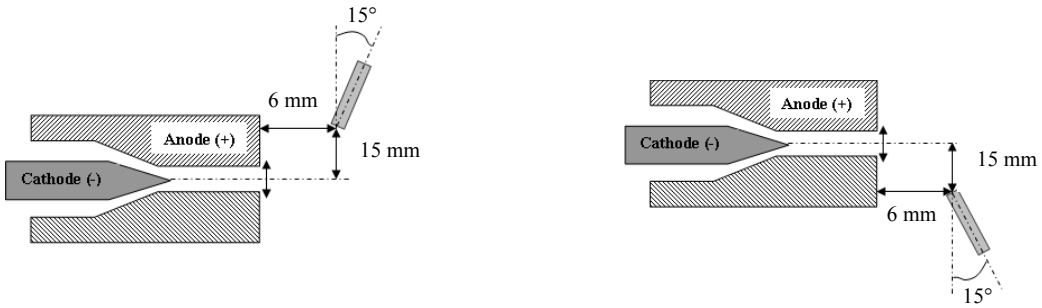

Figure 1: Schema of the suspension injection position in front of the plasma torch

Partially yttria stabilized zirconia (PYSZ) with 8 wt. % Y_2O_3, provided by Inframat Corp. (Willington, CT, USA), was sprayed. The powder particle size ranged between 30 and 60 nm. The powder was mixed with distilled water and ultrasonically and mechanically stirred to break up the

agglomerates. The solid concentration in the suspension was 6% by weight without any dispersant since no sedimentation was observed during a time exceeding the deposition time.

3. Interaction between liquid jet and DC plasma flow

This study concerns the introduction of the liquid into the plasma flow. This point is of high importance because it conditions the future treatment of the liquid and particles in the plasma flow. So, two approaches have been used, the first one by experimental imaging of the material in the plasma flow, the second by modelling.

3.1. Experimental approach

Due to the injector position close to the plasma centreline, the liquid stays as a continuous jet (jet diameter = injector jet). When the Rayleigh regime is reached, the jet breaks down in uniform droplets following the Rayleigh equation (droplet diameter= 1.8 x jet diameter) **[6]**.

A preliminary experiment has been carried out: the continuous water jet interacted with an air cross flow (**Figure 2**) and was analysed by shadow imaging technique **[7] [8] [9].** The same experiment has been done by replacing the air cross flow by the DC plasma flow. For the plasma flow, simple calculations (without integrating compressible effect velocity and density gradients) lead to a Weber number around 500 (**Figure 3)** while the air cross flow leads to a Weber number around 250. According to **[10]**, this Weber number defines the low limit of a catastrophic break-up with the stripping of the matter. The fact that the fragmentation shown in the two images (highlighted by the arrows) are quite similar implies that the thermal effects are negligible upon the fragmentation and that the hydrodynamic effects are the first to take into account.

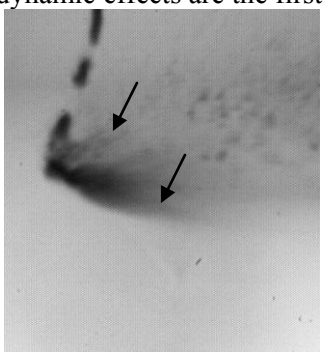

Figure 2: Shadow imaging of water sheet interacting with an air cross flow.

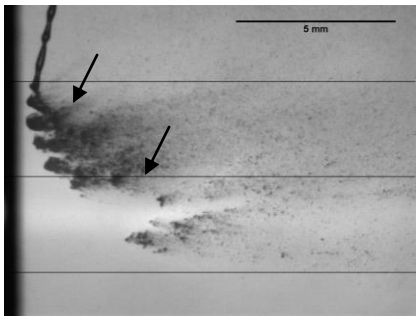

Figure 3: Shadow imaging of water sheet interacting with an argon/hydrogen/helium DC plasma flow.

Two different configurations of water injection (**Figure 1**) have been investigated at different injection pressures (from 0.25 to 0.65 MPa). First, the injector was located below the torch axis (this configuration is called “down to up”) and the liquid flowed up to the plasma jet; then, the injector was located above the torch axis (“up to down”) and the liquid fell down to the plasma jet. Instantaneous images (exposure time of 1µs) are represented in **Figure 4**; the three black horizontal lines represent the jet centreline and the up and down limits of the plasma torch. As expected, an increase in liquid pressure makes the liquid penetrate more easily in the jet. At this point, no significant effect of gravitation seems visible. The introduction of the continuous jet in stair-shape could be due to the unsteadiness of the plasma motion depending on the movement of the electrical arc inside the torch **[5] [11].**

Each instantaneous image has been treated with a low-pass filter to keep only the minimum signal of each image. Then, a new image has been composed by superposing one hundred images to get the shape of the fragmentation zone, **Figure 5** shows the resulting image and therefore the droplets treatment zone in the plasma jet. This figure illustrates the effect of the gravitation: for instance, at

0.65MPa, the “down-to-up” case shows a treatment zone completely integrated in the plasma flow while in the opposite way, the liquid shape trends to get out of the plasma by the bottom.

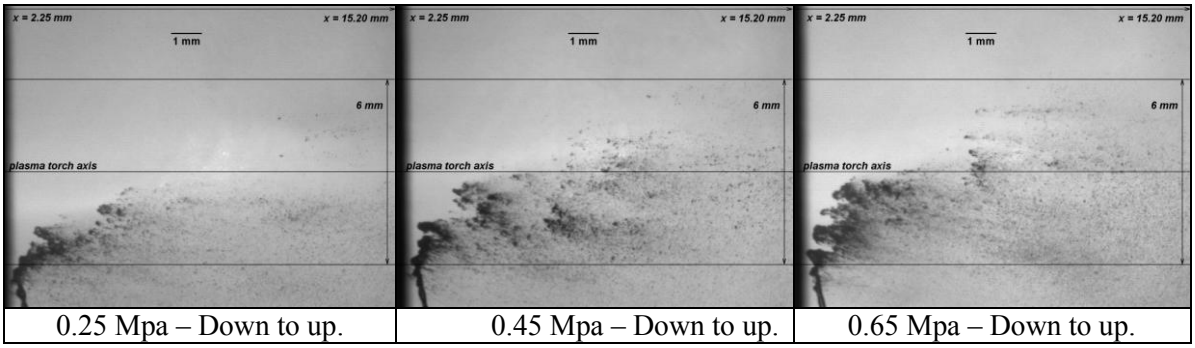

0.25 Mpa – Down to up.	0.45 Mpa – Down to up.	0.65 Mpa – Down to up.

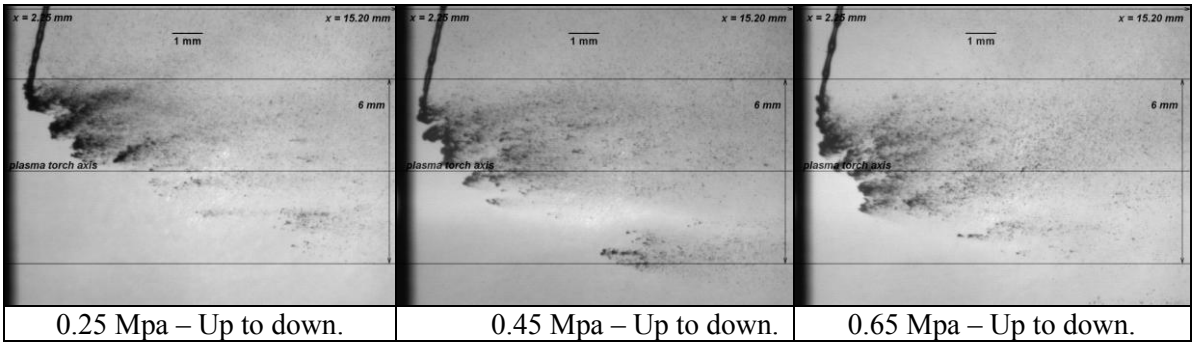

0.25 Mpa – Up to down.	0.45 Mpa – Up to down.	0.65 Mpa – Up to down.

Figure 4: Instantaneous shadow photographs of a continuous water jet interacting with DC plasma flow for different pressures and injection configurations

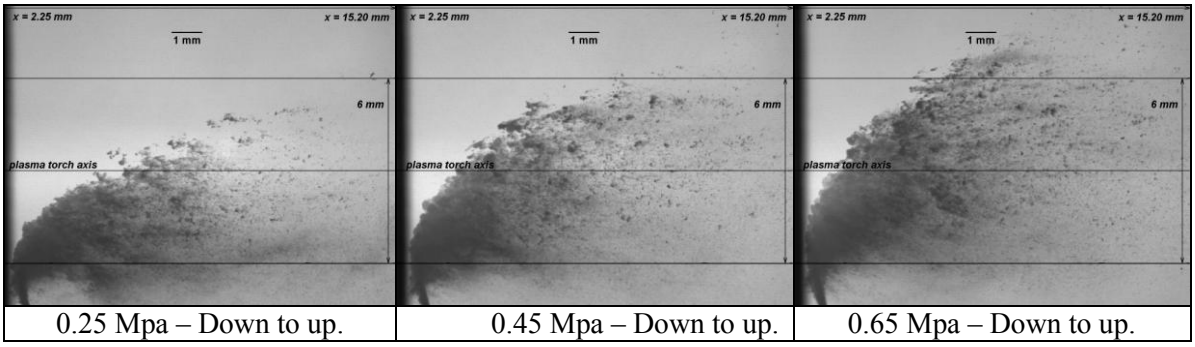

0.25 Mpa – Down to up.	0.45 Mpa – Down to up.	0.65 Mpa – Down to up.

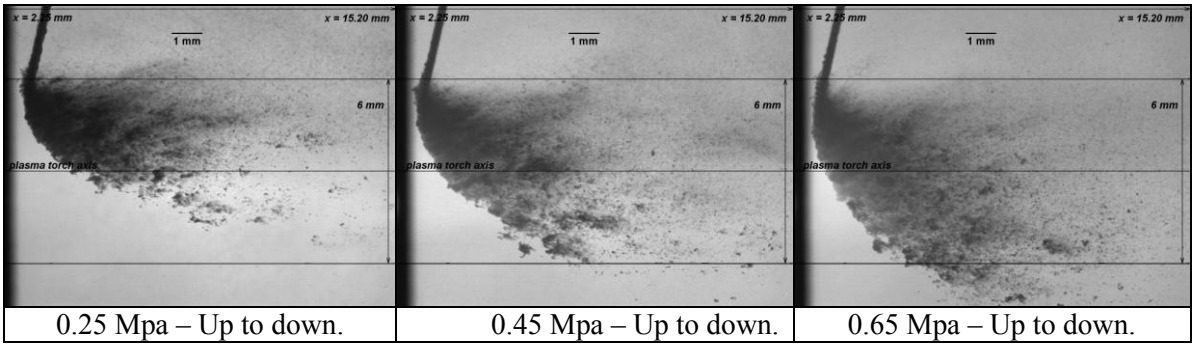

0.25 Mpa – Up to down.	0.45 Mpa – Up to down.	0.65 Mpa – Up to down.

Figure 5: 100 superimposed shadow photographs of a continuous water jet interacting with DC plasma flow for different pressures and injection configurations.

For the other pressure cases, gravitation seems not significant because the liquid has more difficulty to reach the opposite limit of the plasma. From these images, it seems realistic to conclude that most of the particles are in the plasma jet but with a high dispersion. So the next point is devoted to determine if some differences exist between the different configurations of liquid injection.

Each image has been divided in thin slices (200 µm wide) perpendicular to droplet trajectories. In each slice, the maximum of signal intensity has been searched to determine the average maximum trajectory in the jet. The results are represented in **Figure 6**. For all the pressures, the liquid jet is well introduced in the plasma flow (assuming the plasma jet diameter is around the anode diameter in this area). This figure also highlights the difficulty of the liquid to penetrate into the plasma jet depending on the liquid pressure and therefore the difference of particle treatment due to the high gradient of velocity. In the "down-to-up" case, the trajectory does not reach the torch axis whatever the pressure while it does in the opposite way for the upper pressure (more than 0.50 MPa). The difference in trajectory involves different particle treatments in regard to the temperature and velocity zones because of the high gradients of the plasma flow (see **Figure 10** on the **left** side).

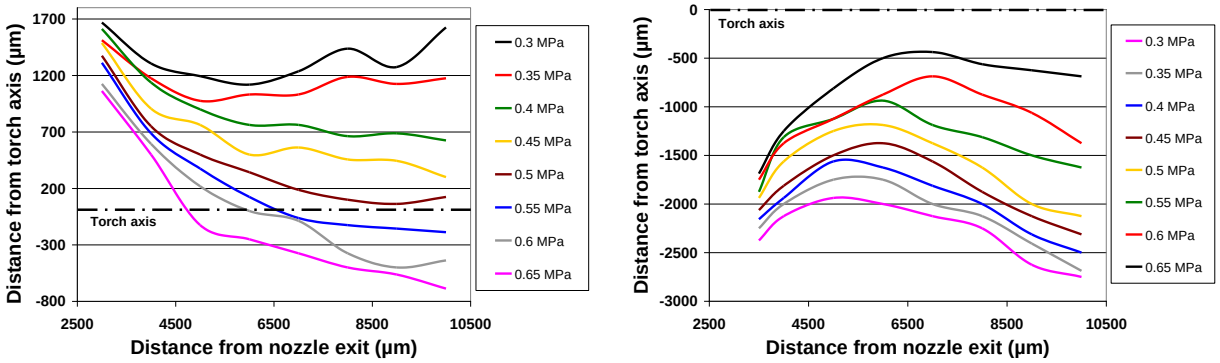

a. Up to down injection

b. Down to up injection

Figure 6: Variation of the maximum of signal intensity downstream of the torch exit

3.2. Model approach

Another way to study the first interactions between the two fluids is to simulate them. This requires getting the convenient tools. Several works have been carried out to develop a multi scale model **[12]**, **[13]** without introducing any analytical models of break-up while other authors analyze the different existing models **[14]**. Here are exposed different kinds of interactions between one single droplet, a train of droplets or a continuous liquid jet and the same DC argon/hydrogen plasma flow. Due to numerous previous investigations in literature **[9], [14], [15],** these works have been carried out with Ar/H2 plasma flow for comparison and validation. Only hydrodynamic effects are taken into account, the thermal one inside the liquid with phase changing is not yet incorporated in the model. The goal is to analyze which way seems the best to introduce the suspension into the jet **[13]**. **Figure 10 left** shows the velocity of Ar/H2 plasma flow and the analysis area where the droplets interact with the plasma. As seen in **Figure 10 left,** the interaction zone of the droplet with the plasma plume is very peripheral with rather low gas velocity, around 250 m/s. So, the individual injected droplets get low Weber number (respectively 5 for a diameter of 75 µm and a velocity of 40 $m.s^{-1}$, then 15 for a diameter of 200 µm and 30 m/s for the injection velocity).

First, two alone droplets are injected close to the plasma jet (respectively **Figure 7** and **Figure 8**). These classic cases correspond to a fragmented liquid jet from an injector diameter of about 40 and 110 µm respectively according to the Rayleigh-Plateau theory **[6]**. In **Figure 7,** due to the important surface tension forces, a bag is formed around the droplet and is fragmented into several secondary droplets with a mean diameter of about 8 µm. In **Figure 8,** the initial droplet is stretched and the formation of a thin film with surface waves is observed. As no thermal effect is taken into account in

the liquid, this film stays at the surface of the gas flow without evaporation. Its thickness is about 3 µm. Then, the film is fragmented into small secondary droplets, but these droplets stay again at the boundary of the plasma flow and seem not more penetrating into the jet.

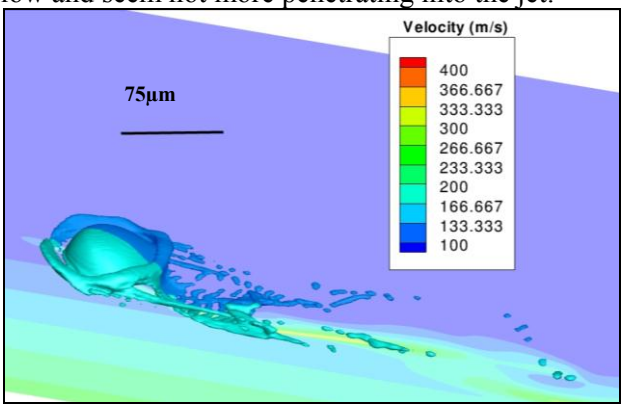

Figure 7: Velocity field (m/s) around the water droplet at $t=5.10^{-6}$s (We=5)

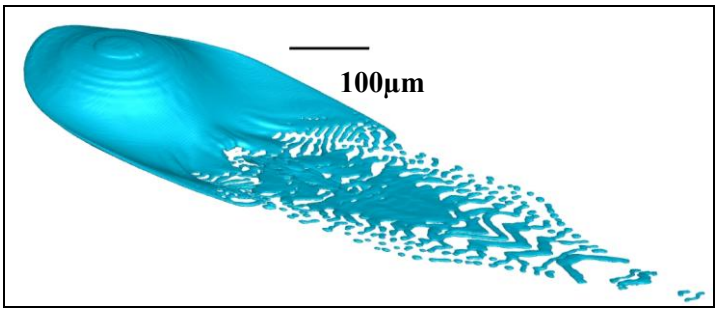

Figure 8: Shape of 200 µm primary droplet interacting with the plasma flow (We=15)

For the train of droplets, several identical droplets are injected. The injection frequency is about 22 10^4 droplets/second. In **Figure 9**, the droplets seem to have again difficulty to penetrate the plasma but the high introduction frequency involves an increase in interaction between the droplets issued from the fragmentation and the plasma flow: this leads to trajectories closer to the plasma axis. This can be seen at the bottom-left with the smallest droplets which disperse in the flow. At this point, the thermal effects in the liquid have to be included in the model to evaporate the water involving ceramic particles flight. This image highlights the necessary mass effect due to numerous-primary-droplets injection to facilitate the penetration of the secondary droplets in the flow.

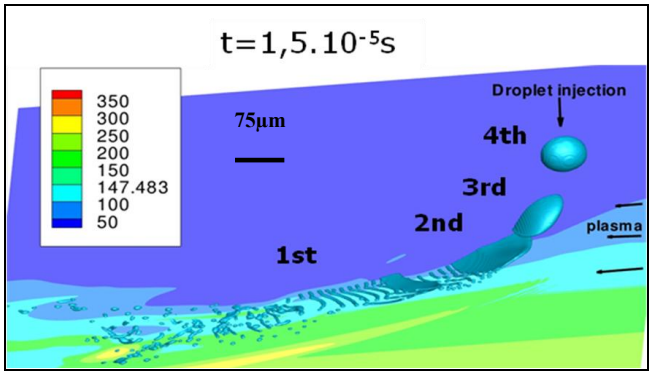

Figure 9: Velocity field (m/s) at $t=1.5.10^{-5}$s (We=5) for multi-droplet injection.

For the continuous liquid sheet injection, the calculation domain was changed and it was a box of dimension 10 mm × 5 mm × 5 mm. As seen in **Figure 10 right**, the penetration of the liquid into the plasma is quite easier: the liquid column reaches nearly the plasma torch axis with some distortions and begins to break up in large droplets. It should be noted that the calculation domain involved more than 1.5 million of meshes to correctly model the fragmentation and get small droplets.

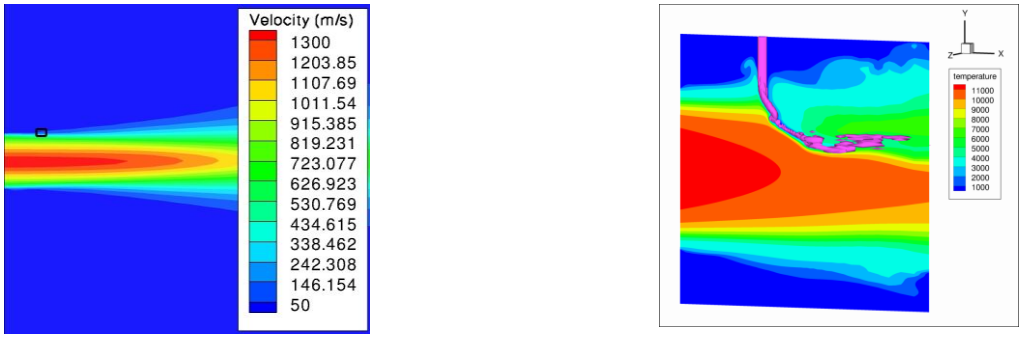

Figure 10: Plasma velocity (m/s) and investigation zone for singular droplets analysis (left) and temperature field (K) for a continuous liquid jet interacting with Ar/H_2 plasma flow (right).

To conclude this part, it seems easier to use a continuous liquid jet to carry on the suspension into the plasma flow core in order to get an efficient treatment of the liquid and therefore, of the ceramic particles. Big droplets, or continuous jet, bring more liquid matter which takes more time to evaporate in contrary of small droplets that evaporate rapidly and so cool down the plasma in a shorter time. So, the plasma plume properties will be completely different depending on the type of liquid injection and fragmentation. This will be confirmed in the next part with the experimental approach.

4. Coating properties.

Coatings have been realized under **Table 1** conditions at a spraying distance of about 40 mm. The substrate surface temperature was about 400°C at the beginning of the spray process, it was monitored by an infrared pyrometer (Modeline 4, Ircon, 8-14 µm wavelength range) and controlled during the spray process by CO2 cryogenic cooling to maintain the substrate temperature close to 400 °C.

4.1. Coating architecture and thickness.

The microstructures of coatings were observed by Scanning electron microscopy (SEM, Philips XL30), either with secondary electron (SE) or back-scattered electron (BSE) modes. The thickness of each coating has been estimated from SEM micrographs (ten measurements).

The architecture of coatings looks like that of **Figure 11** whatever the position of the injector for the constant injection pressure.

The only effect of the liquid injection parameters concerns the coating thickness (**Figure 12**) with a higher deposition efficiency rate for the down-to-up position which decreases when the pressure rises up to 0.6 MPa. These different results can be compared with the mean trajectories of the particles which are presented in section **3.1.** In fact, for the down-to-up injection, more particles seem to stay in the plasma flow than for the up-to-down injection. So more particles are correctly heated and accelerated and so the deposit rate is higher. Concerning the highest liquid injection pressure, a part of the particles goes out of the plasma jet, so fewer particles participate to the coating generation.

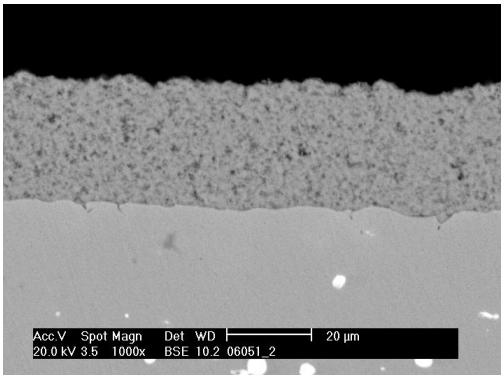

Down-to-up injection at 0.6 MPa

Figure 11: SEM micrograph of coating obtained on BSE mode

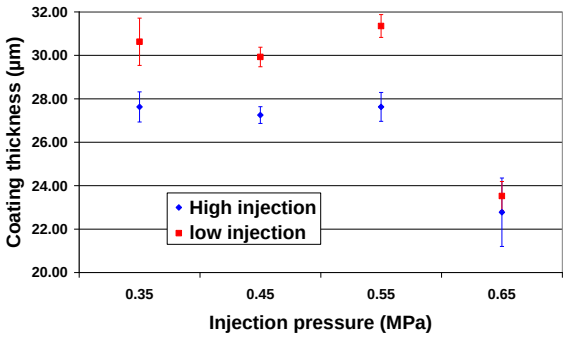

Figure 12: Variation of coatings thickness versus injection pressure for two configurations

4.2. Surface topography.

Surface roughness has been measured using a surface roughness tester (Perthometer PGK 120). The average roughness Ra, defined as the arithmetic mean of the profile irregularities from the mean line, is used to quantify the coating surface roughness. The relationship between coating surface roughness values and liquid injection pressure is illustrated in **Figure 13:** the average roughness decreases with the liquid injection pressure. The coating surface state is a consequence of the pilling-up of the lamellae. The decrease in roughness with pressure indicates differences in particle velocity at impact, and thus differences in particles thermal treatment in the plasma jet.

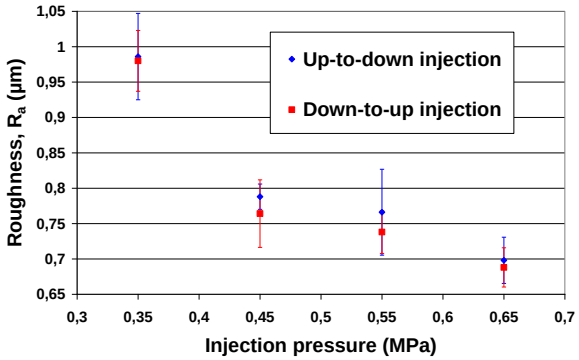

Figure 13: Relationship between coating surface roughness and liquid injection pressure

As seen in **Figure 6**, when the injection pressure increases, more particles reach higher gas temperature and velocity zones close to the plasma jet axis leading to a more complete thermal treatment. So the coating surface is more homogeneous. But this seems contrary with the architectures which are identical for all coatings (**Figure 11).** The particles, which take part in the coating, result from droplets with trajectories close to the torch axis. In fact, the droplet dispersion in the plasma jet is important and only a percentage of the droplets are sufficiently treated and produce nanometre size particles that flatten on the substrate with high velocities. For the pressure range, there are always enough particles in the control zone to build a coating and the microstructures look alike. On the other hand, coating thickness and roughness which depend on the particle size are more sensitive to liquid injection pressure.

4.3. Mechanical properties.

The mechanical properties of the coatings have been evaluated by two techniques: nano- indentation and classical Vickers Hardness test. The nano-indentation has been performed on the polished cross section of samples, in the conditions described in **[2]**. The results are presented in **Table 2**. Whatever the injection configuration and parameters are, the values are in the same range showing no difference of hardness and Young Modulus between the coatings. This agrees with the coating morphology observations.

	Up to down injection				Down to up injection			
Liquid injection pressure (MPa)	**0.35**	**0.45**	**0.55**	**0.65**	**0.35**	**0.45**	**0.55**	**0.65**
Coating hardness (GPa)	9.1 ± 1.4	9 ± 0.8	8 ± 1.4	8.5 ± 0.6	8.8 ± 1	10.1 ± 1.1	9 ± 1.2	8.5 ± 1.2
Coating Young's modulus (GPa)	140 ± 14	136 ± 8	139 ± 9	135 ± 8	141 ± 9	158 ± 11	139 ± 10	137 ± 12

Table 2: Coating mechanical properties from nano-indentation technique

Then Micro-Vickers indentation test has been performed on the top of the coating: it reveals a slight difference between the up-to-down and the down-to-up injection. This difference might be due to the difference of the coating thickness. In fact, the indentation depth is high in comparison to the thickness of coatings and so, the hardness of the substrate can play a role during the test. A mathematical model, presented in **[16]**, gives the possibility to adjust the hardness value by the Jönsson and Hogmark model **[17]**:

$$H_m = H_s + (2c\frac{t}{d} - (c\frac{t}{d})^2) \times (H_f - H_s)$$

Where H_m is the measured coating hardness, H_s the substrate hardness, H_f the real hardness, t the coating thickness, d the Vickers print diagonal and c a constant, (0.5 for fragile materials, 1 for ductile ones). By using the value of 0.5 for c, the results are in the same range than the values obtained by nano indentation, with no effect of the suspension injection parameters (**Table 3)**.

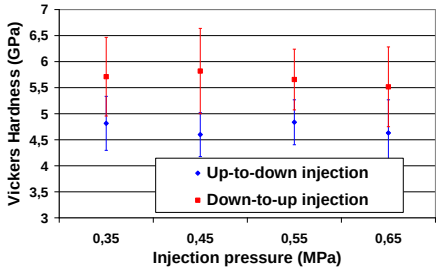

Figure 14: Coating hardness from Vickers indentation test on the top of the coating

	Up to down injection				Down to up injection			
Injection pressure (MPa)	**0.35**	**0.45**	**0.55**	**0.65**	**0.35**	**0.45**	**0.55**	**0.65**
Hardness (GPa)	8.89	8.98	8.84	9.33	10.27	10.42	9.86	10.79

Table 3: Vickers Hardness values adjusted by using the Jönsson & Hogmark model

5. Conclusion.

Investigations upon manufacturing of YSZ coatings by suspension plasma spraying have been carried out. The interactions between the liquid jet and the DC plasma flow were analyzed both by numerical simulation and measurements. Instantaneous and average images of the liquid by shadow imaging techniques showed the break-up modes and the difficulty of penetration depending on the injection pressure and configuration. From these images, average droplet trajectographies were extracted highlighting difference behaviors inside the plasma flow: reaching the plasma axis required high pressures and up-to-down injection configuration. By modeling, comparison of interaction between,

one singular droplet, droplets train or continuous liquid jet and the plasma flow showed a better penetration into the plasma jet with continuous sheet due to a necessary mass effect.

Finally, coating deposition was discussed: all the coatings showed the same microstructure while the particles treatment in the plasma depended on the penetration zone. The only parameter sensible to the penetration was the deposition efficiency rate which depended on the injection pressure: a too high pressure (higher than 0.6 MPa) led to a decrease in of the deposition efficiency rate. These investigations showed that suspension plasma spraying is a "robust" process able to generate coatings with correct mechanical properties even if the penetration of the suspension was not well controlled. This implies nevertheless that the liquid pressure is sufficient to make part of the suspension penetrate into the plasma jet.

References

[1] J. BOUCHARD and R. BENNETT, Generation IV International Forum, published in Energy Focus Spring 2009

[2] R. VERT, D. CHICOT, C. DUBLANCHE-TIXIER, E. MEILLOT, A. VARDELLE, G. MARIAUX, Adhesion of YSZ suspension plasma-sprayed coating on smooth and thin substrates, Proceedings of RIPT and S2TS 2010, LILLE, Surf. Coatings Tech., accepted, in press.

[3] S.JANISSON, A.VARDELLE, J.F. COUDERT, P. FAUCHAIS, E. MEILLOT, Analysis Of The Stability Of Dc Plasma Gun Operating With Ar–He–H2 Gas Mixtures, in: Annals of the New York Academy of Sciences, 891 (1999), pp. 407–416.

[4] DUAN Z., HEBERLEIN J., Arc Instabilities in a Plasma Spray Torch, J. Thermal Spray Technology 11 (1) (2002) pp. 44–57.

[5] J. FAZILLEAU, C. DELBOS, V. RAT, J.F. COUDERT, P. FAUCHAIS and B. PATEYRON, Phenomena Involved in Suspension Plasma Spraying. Part 1: Suspension Injection and Behavior, Plasma Chem. Plasma Process, 26 (2006) pp. 371-391.

[6] L. RAYLEIGH, Proc. R. Soc. Lond., 29 (1879) pp 71-97.

[7] LaVision GmbH, Anna Vandenhoeck Ring 19, 37081 Goettingen, Germany, www.lavision.com.

[8] D. DAMIANI, S. GOUTIER, R. VERT, M. VARDELLE, Proceedings of Congrès Francophone de Techniques Laser, CFTL 2010, Vandoeuvre les Nancy, Sept 2010, France (in french), in press.

[9] C. MARCHAND, C. CHAZELAS, G. MARIAUX and A. VARDELLE, Liquid precursor plasma spraying: observation of liquid feedstock break-up, proceedings of International Thermal Spray Conference: Thermal Spray Crossing Boarders - ITSC 2008, Maastricht, Netherlands, June 2-4 2008, ISBN 978-3-87155-979-2

[10] M. PILCH and C.A. ERDMAN, Use of breakup time data and velocity history data to predict the maximum size of stable fragments for acceleration-induced brakup of a liquid drop, Int. J. Multiphase Flow, 13 (6) (1987) pp 741-757.

[11] P. FAUCHAIS, R. ETCHART-SALAS, V. RAT, J.F. COUDERT, N. CARON, and K WITTMANN-TENEZE, Parameters Controlling Liquid Plasma Spraying : Solutions, Sols or Suspensions, J. Thermal Spray Technology 17 (1) (2008) pp 31-58

[12] S.VINCENT, G. BALMIGÈRE, J.-P. CALTAGIRONE and E. MEILLOT, J. Comput. Phys. 229 (2010) 73-106.

[13] C. CARUYER, S. VINCENT, E. MEILLOT and J.P. CALTAGIRONE, Modeling the first instant of the interaction between a liquid and a plasma jet with a compressible approach, Proceedings of RIPT and S2TS 2010, LILLE, Surf. Coatings Tech., accepted, in press.

[14] C. MARCHAND, A. VARDELLE, G. MARIAUX, P. LEFORT, *Modelling of the plasma spray process with liquid feedstock injection*, (2008) Surf. and Coatings Tech., 202 (18), pp. 4458-4464

[15] R. ETCHART-SALAS, V. RAT, J.F. COUDERT, P. FAUCHAIS, N. CARON, K. WITTMAN, and S. ALEXANDRE, Influence of Plasma Instabilities in Ceramic Suspension Plasma Spraying, J. Thermal Spray Technology 16 (5-6) (2007), pp.857- 865..

[16] D. CHICOT and J. LESAGE, Absolute hardness of the films and coatings, Thin Solid Film, 254 (1995), pp.123-130

[17] B. JÖNSSON and S. HOGMARK, Hardness measurements of thin films, Thin Solid Films, 114 (3) (1984), pp. 257-269